THE ASTROPHYSICAL JOURNAL, 463:326–335, 1996 May 20

ADAPTIVE OPTICS IMAGING OF GG TAURI: OPTICAL DETECTION OF THE CIRCUMBINARY RING

C. RODDIER, F. RODDIER, M. J. NORTHCOTT, J. E. GRAVES, AND K. JIM
Institute for Astronomy, University of Hawaii, 2680 Woodlawn Drive, Honolulu, Hawaii 96822;
croddier, roddier, north, graves@galileo.ifa.hawaii.edu
Received 1995 August 25; accepted 1995 December 4

ABSTRACT

High angular resolution images of GG Tau have been obtained in the *I*, *J*, *H*, and *K* bands with the University of Hawaii adaptive optics system. The close binary pair is found to be near periastron, and it rotates clockwise. It consists of a K7-M0 star with an M4 companion. Masses inferred from dynamical motion are larger than the spectral type suggest. The companion appears to be younger than the main star. Both stars seem to be surrounded with a warm unresolved disk. Images reveal a circumbinary ring also recently detected at millimetric wavelengths. The ring seems to be produced by light scattered by the edge of a cavity inside a much larger disk. At the cavity edge, the disk thickness is estimated to be one-tenth of the cavity radius. Light which illuminates this cavity edge appears to be reddened by absorption through the inner disks. Azimuthal variations of the illumination indicate that the inner disks must be lumpy.

Subject headings: circumstellar matter — infrared: stars — stars: individual (GG Tauri) — stars: pre–main-sequence

1. INTRODUCTION

During the last decade, there has been growing evidence that T Tauri–type stars are surrounded with circumstellar disks (Strom, Edwards, & Strom 1989a). Data from *IRAS* have shown that most of them have an excess emission in the far-infrared, indicating the presence of an optically thick dust envelope. Myers et al. (1987) have argued that, since these stars are visible at shorter wavelengths, the envelope cannot be distributed isotropically, but rather is distributed in the form of circumstellar disks. In the near-infrared, maximum entropy deconvolution (Grasdalen et al. 1984) and speckle interferometry techniques (Beckwith et al. 1984) have provided evidence for halos around some of the objects. The most compelling evidence comes from millimetric observations (Koerner, Sargent, & Beckwith 1993; Skrutskie et al. 1993). Interferometric arrays have produced maps of the molecular gas distribution and velocity around T Tauri stars with a resolution of a few arcseconds. In several cases (HL Tau, GG Tau), the gas is clearly distributed in an elongated structure moving around the star in Keplerian orbits (Sargent & Beckwith 1987; Simon & Guilloteau 1992; Kawabe et al. 1993; Kitamura et al. 1993; Dutrey, Guilloteau, & Simon 1994). Images of HL Tau and T Tau have been taken recently by the *Hubble Space Telescope* (*HST*) (Staplefeldt et al. 1994). They show that, in the visible, HL Tau is totally hidden inside a nebula, whereas a bright arc of scattered light can be seen close to T Tau. Both observations are consistent with light scattered by a circumstellar disk. We present here near-infrared images of GG Tau obtained with adaptive optics. GG Tau is a quadruple system (Leinert et al. 1991). in the observations described here, all four components were imaged on the same field of view. The two north components form a close pair with an angular separation of about 0.″25. Our images reveal that this pair is surrounded with a bright elliptical ring about 3″ long in agreement with the most recent millimetric observations (Dutrey et al. 1994). We discuss the result of astrometric and photometric measurements made on these images.

2. DATA ACQUISITION AND PREPROCESSING

Data presented here were obtained with a new Cassegrain-focus adaptive optics instrument built at the Institute for Astronomy (University of Hawaii). The instrument consists of a 1024 × 1024 pixel CCD camera, a 1024 × 1024 pixel HgCdTe infrared camera recently built by Hodapp and his coworkers, and a real-time atmospheric compensation device, or adaptive optics (AO) system. The AO system is an improved version of the experimental AO system already described in the literature (Roddier, Northcott, & Graves 1991; Roddier et al. 1994). The instrument was mounted at the Cassegrain f/36 focus of the Canada-France-Hawaii Telescope (CFHT), and the observations took place during the night of 1994 December 23. For the infrared images, the magnification is 0.″035 per pixel which gives us a field of view of 35.″8 × 35.″8. For the CCD images, the magnification is 0.″024 per pixel, and the field of view 24.″6 × 24.″6.

Our GG Tau data consist of three sets of frames taken with the IR camera: a set of 15 frames taken through a standard *J* filter with exposure times ranging from 5 to 10 s, a set of 13 frames taken though a standard *H* filter with exposure times ranging from 3 to 7 s, and a set of 10 frames taken though a standard *K* filter with exposure times of 2 s. A fourth set of 20 frames was taken with the CCD camera through a narrow-band filter centered at 0.85 μm, with an exposure time of 60 s. Between each exposure, an offset mirror was tilted to move the image on the camera, while keeping it on the wave front sensor. This was done to minimize the effect of bad pixels or inhomogeneities in the detector response. It also allowed us to estimate the sky background from the same set of frames. Similar sets of data were obtained on nearby reference stars both before and after the object data. Those taken before were obtained on a star slightly brighter than GG Tau; that is, the wave front sensor was receiving more photons and delivering slightly less noisy signals. Those taken after were obtained on a star of similar red magnitude, so that the wave front sensor response was about the same as that on GG Tau.

What we call data preprocessing consists of the estimation and subtraction of the background, bad pixel elimination, intensity normalization, and frame recentering and averaging. The background was subtracted first. A few bad pixels were then eliminated by replacing their intensity value with an average of that of the neighboring points. Intensity normalization was done by equating the flux in the central source to that of a theoretical diffraction-limited point-spread function (PSF) with maximum intensity equal to unity. When this is done on reference frames, the maximum intensity becomes equal to the Strehl ratio. Frame recentering was done in two steps. First we looked for the brightest pixel in each image and used it as a first estimate of the center. Then we took the Fourier transform of the image and displayed a map of the phase of the Fourier transform. We found that the phase was well determined inside an area extending up to the diffraction limit of the telescope. Taking an area only slightly smaller, we made a two-dimensional linear fit to the phase map, subtracted the linear terms, and took the inverse Fourier transform of the new complex amplitude. By doing this, the new image center becomes the center of "gravity" of the intensity distribution. We believe that by using this procedure we can determine it within a fraction of one pixel. Averaging of the recentered frames was done by taking the median rather than the mean.

3. IMAGE DECONVOLUTION

All our compensated images were deconvolved further using PSFs derived from similar data taken on nearby reference stars. After a few trials with various algorithms, we finally settled and used the Lucy-Richardson algorithm which appeared to best suit data with a very high dynamic range such as ours.

Photometry is known to be difficult on deconvolved images. To gain confidence in the photometric quality of our deconvolved images, we performed the following tests. We took from the preprocessed but undeconvolved image a 256×256 pixel subframe centered on the object and a 256×256 subframe containing pure sky background. The subframe containing the object was attenuated by factors ranging from 0.01 to unity and added to the sky background frame. The resulting image was then deconvolved and the illumination measured over 3×3 pixels areas in the attenuated image. For each of these areas, we plotted the measured illumination as a function of the attenuation coefficient on a log-log scale. This gave us a series of curves (one per area) shifted horizontally. Removing the shift produced a single curve; most of it was straight with a slope unity. Departure from linearity was found to occur only at the faintest levels. This photometric calibration curve was found to be quite insensitive to the parameters of the deconvolution algorithm (noise and background estimates), except at these low levels at which parameters could be adjusted for best linearity. These optimized parameters were used in the data reduction.

Using the same series of attenuated images with known attenuation, we also tested the convergence of the iterative deconvolution process by plotting the measured intensity as a function of the number of iterations. We found three different patterns of evolution we call poor convergence, fair convergence, and good convergence. Poor convergence was observed when the intensity was below some threshold. Then it kept decreasing at each iteration and converged toward zero even though we knew there was some "signal" in our attenuated images. Fair convergence was observed in areas which are brighter than the threshold, but are surrounded with other areas which are below the threshold. In this case, the intensity decreased reached a minimum, and then increased without actually converging. The minimum is usually reached after 10–15 iterations and is close to the value one would obtain for nonattenuated images. In the data reduction process, we took this minimum as our flux estimate. Good convergence was observed in all other cases. However, the required number of iterations was found to depend upon the intensity level. Faint areas away from the central stars required 10–20 iterations, whereas brighter areas near the central stars required more than 100 iterations. The most accurate results were obtained in the H band because images are better compensated for than in the J band and data are less noisy than in the K band. Less accurate results were obtained in the K band because of the thermal background noise.

The most critical step in the deconvolution process was found to be the choice of the PSF. As stated above, PSFs were estimated from data taken on reference stars both before and after the source data. Although all the deconvolved images display the same broad features, details vary from one image to another depending on the PSF being used, and it is difficult to decide which ones are trustworthy. The most striking feature seen on all the images is the elliptical ring (Figs. 1–3 [Pl. 22–24]). This is clearly not an artifact. All the H-band images show the entire ring. All the J-band and K-band images show at least the brightest part of the ring on the north-east side. Therefore, we decided to use the ring visibility as a quality criterion for the reconstructed images and select the PSFs accordingly. PSFs essentially consist of three parts:

1. A narrow diffraction-limited core, the same on all the images. Only its intensity varies somewhat from one image to another, mainly in the J and H band.
2. The first two diffraction rings. These are the most affected by residual aberrations. They show evidence for some residual astigmatism and triangular coma and vary from one image to another except in the K band, where all the images are well compensated.
3. The wings produced by the residual uncompensated turbulence. They are very similar from one image to the other but are sensitive to noise.

The best results were obtained by constructing composite PSFs, the wings of which were obtained by taking the median of all the available reference images. By doing this, we reduced the noise level to a minimum. For the core and the first diffraction rings, we considered two options. One option was to take them from the sharpest (higher Strehl ratio) reference star images, which were recorded immediately before the GG Tau data, on a star brighter than GG Tau. The other option was to take those recorded immediately after the GG Tau data, on a star of similar brightness. Since we had only a few such frames, we also added the sharpest images of the brighter south component of the GG Tau quadruple system to form the core and the first rings of the PSF. This gave us what we believe to be a well-matched PSF. Both sets of deconvolved images are shown in Figures 1–3. As one would expect, images deconvolved with the sharpest PSF show fewer details but are less noisy. Images deconvolved with a matched PSF show more details but are

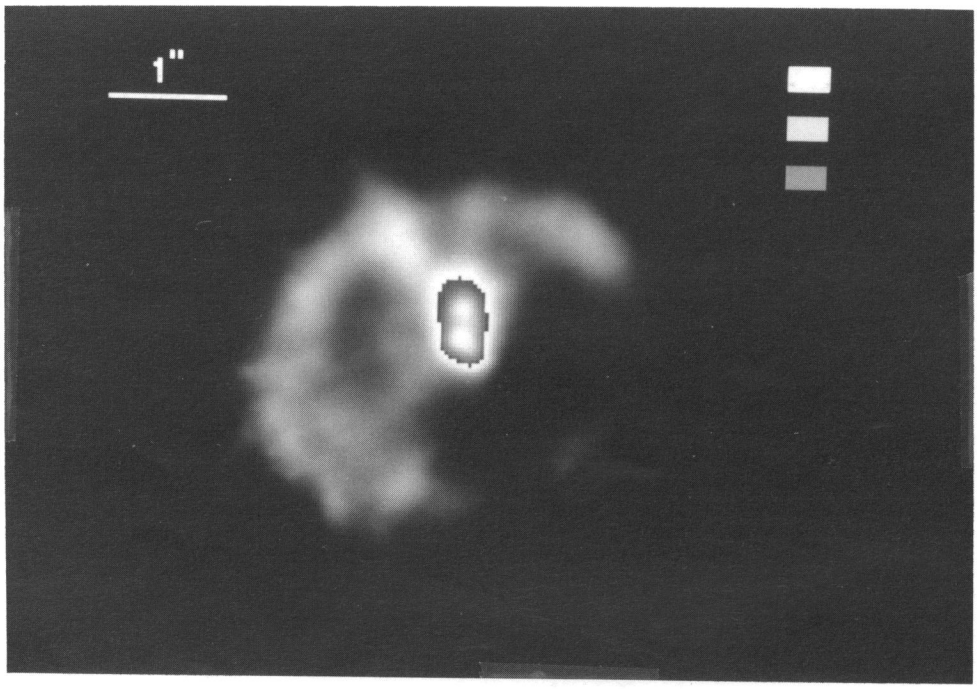

FIG. 1*a*

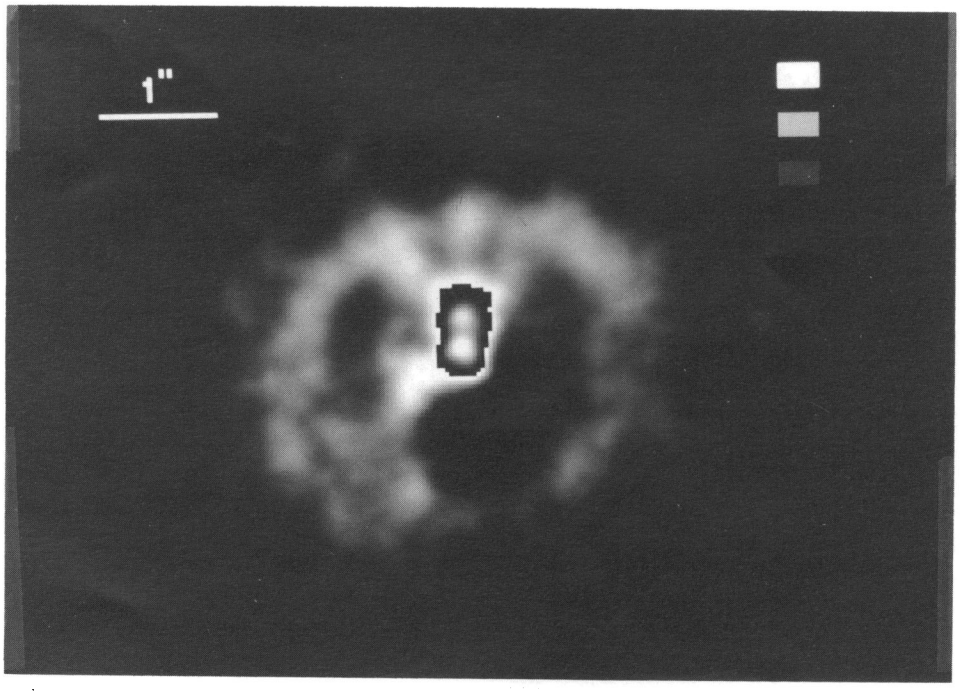

FIG. 1*b*

FIG. 1.—*J*-band image deconvolved with (*a*) a sharp PSF and (*b*) a matched PSF. Maximum intensity has been normalized to unity. Intensity levels 10^{-3}, 10^{-4}, and 10^{-5} are indicated in boxes in the upper right corner. All intensities larger than 10^{-3} have been divided by 10^{3}.

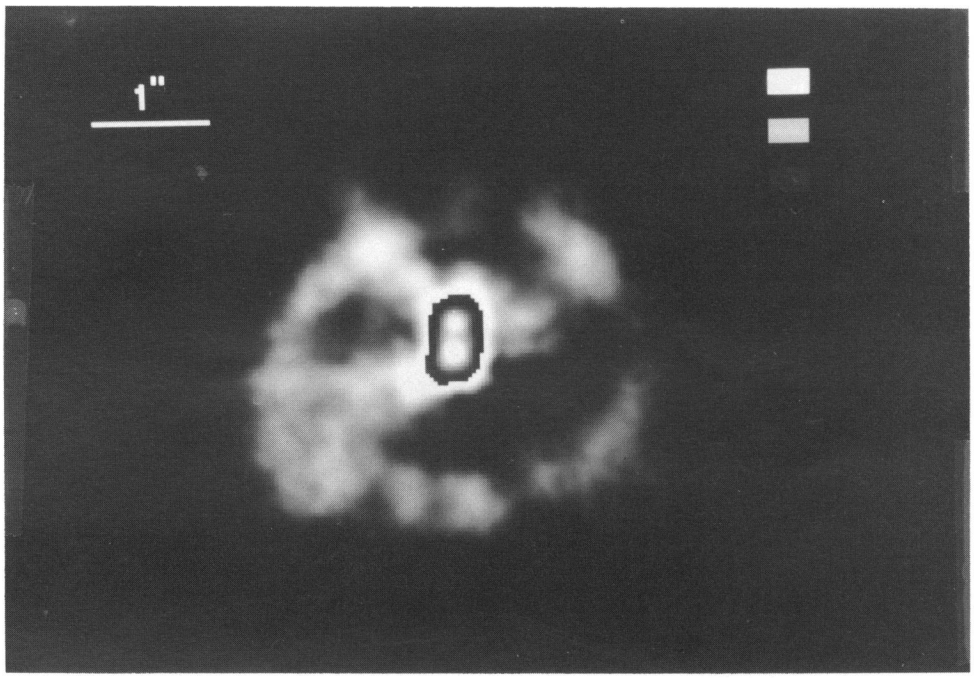

FIG. 2*a*

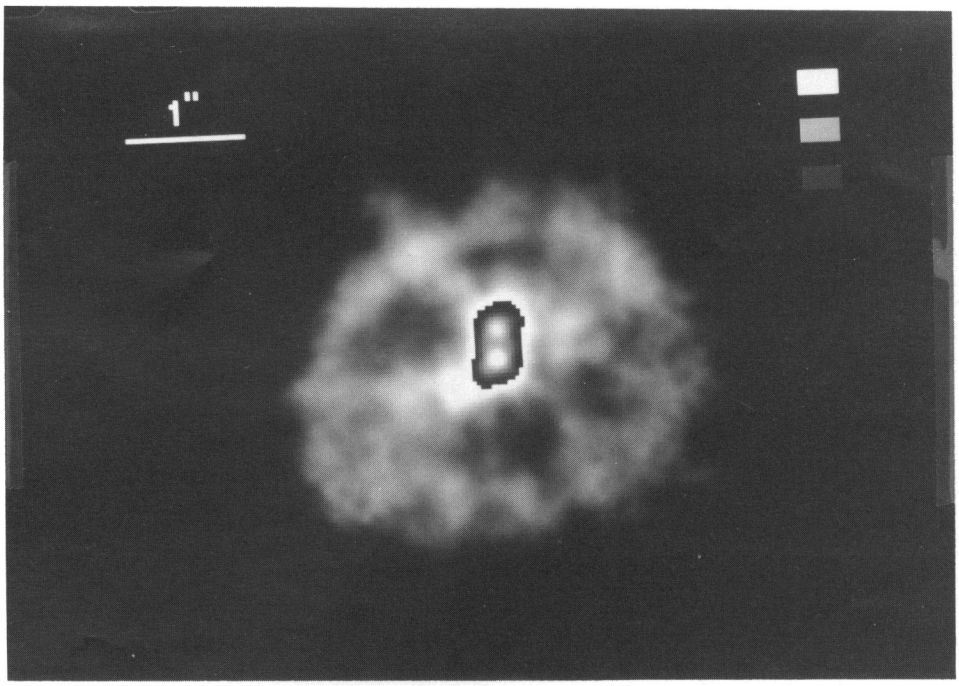

FIG. 2*b*

FIG. 2. Same as Fig. 1, but in the *H* band

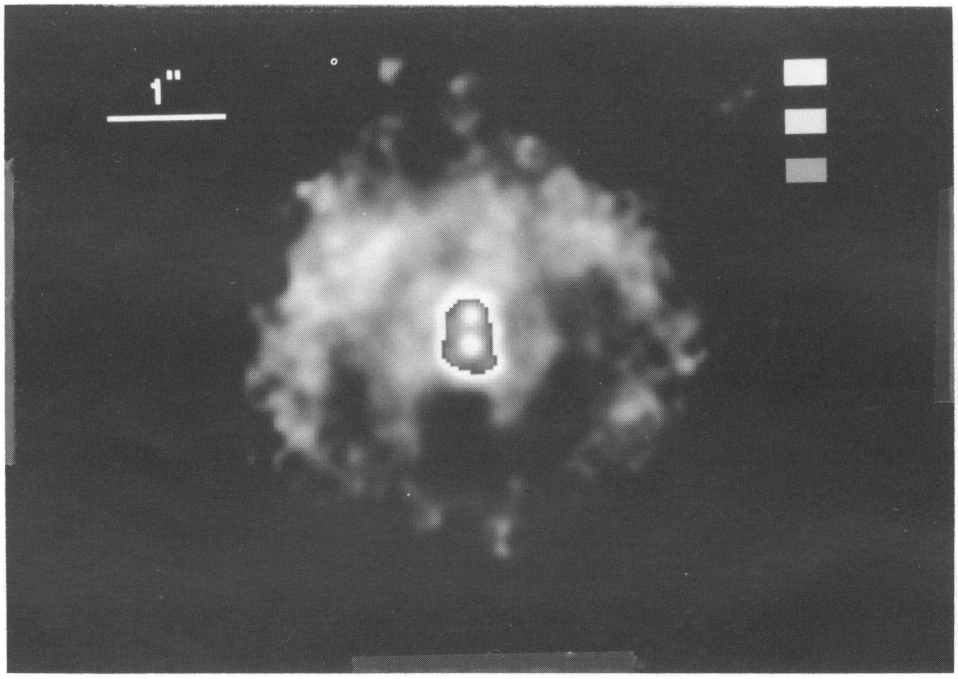

FIG. 3*a*

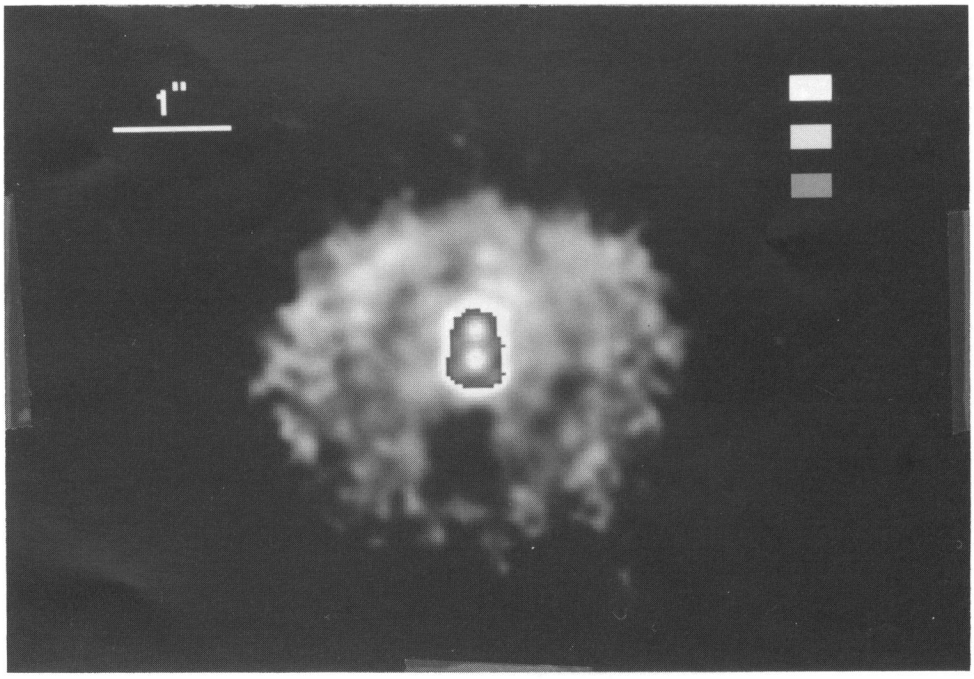

FIG. 3*b*

FIG. 3. Same as Fig. 1, but in the *K* band

noiser. They also show a larger amount of light scattered close to the central stars.

For the GG Tau data themselves, we adopted a similar procedure; that is, we made a composite image with two different areas. Inside a small area encircling the binary star, we used only the sharpest images. Outside this area, we took the median of all the available data. The reconstructed images shown in Figures 1–3 were obtained with these composite images.

4. IMAGE DESCRIPTION

Because of the very large dynamic range involved, the images are difficult to reproduce. We have reproduced only *J*-, *H*-, and *K*-band images (Figs. 1–3). In all cases, the maximum intensity has been normalized to unity. Then, to reduce the dynamic range, all the intensities above 10^{-3} have been divided by 10^3. Gray levels corresponding to intensities of 10^{-3}, 10^{-4}, and 10^{-5} are displayed in small rectangular boxes in the upper right corner of each image. For the display itself, we used a power law with exponent 0.3 for the *J*-band images and 0.4 for the *H*- and *K*-band images.

The images show several features that we describe briefly. First is the binary star. It is clearly resolved even on raw data, including those taken with the CCD camera. As we shall see, the position angle and angular separation agree well with those published in the literature. The second most important feature is an elliptical ring surrounding the binary pair. Its dimensions are about $3''.1 \times 2''.6$. It can be seen on all the *J*, *H*, and *K* deconvolved images, but not in the CCD images. The southwest side, which is fainter than the northeast side, appears only partially on some *J* and *K* images. However, fine tuning the PSF as described above makes it appear entirely. A similar feature of the same size has been recently observed at millimetric wavelength (Dutrey et al. 1994) and identified as the outer rim of a cavity produced by tidal forces in a circumbinary disk (Lin & Papaloizou 1993; Artymowicz & Lubow 1994, 1995). As we shall see, the dimensions and orientation of the ring are in excellent agreement with millimetric observations. A third feature is a bright spoke extending from the central stars to the ring in a northeast direction at a position angle of about 35° from north. It appears mainly in the *J* and *H* bands, but it is also seen on the CCD images. Its intensity depends on the PSF being used for deconvolution. To check for possible artifacts, we have systematically deconvolved one PSF with another. Owing to some residual astigmatism, a similar feature does occasionally appear, but with much less intensity. Therefore, we believe that this feature is real but, because of residual aberrations, its intensity is difficult to determine. We have interpreted this feature as a beam of light shining through a hole in an inner circumstellar disk. Other features can also be seen inside the cavity, especially in the images deconvolved with a matched PSF. For instance, the cavity appears to be systematically brighter in the southeast quadrant. This may be due to material streaming from the ring toward the central stars, as recent simulations suggest (Artymowicz & Lubow 1995). There are also indications of a similar effect in the opposite (northwest) quadrant. Features close to the central stars are the most affected by residual aberrations and are considered as unreliable. Artifacts due to incomplete cancellation of light diffracted by the telescope spider arms are also clearly seen. We have avoided making photometric measurements in these areas. The wavy structure seen in the *H* band along the south part of the ring is intriguing and may be real (Fig. 2*b*).

5. ASTROMETRY

5.1. *Close Binary*

We have measured the angular separation and the position angle of the close binary both on the data presented here, and on data obtained in 1993 December with an earlier version of our adaptive optics system. The results are presented in Table 1, together with other results which have been published in the literature. Our 1993 December measurements were calibrated using two binaries with a known orbit, α Gem and α Psc (Roddier et al. 1995). For the 1994 December measurements, we took the two south components as calibrators, using the angular separation and position angle published by Leinert et al. (1993). Because these stars are on the same frame, they provide a convenient reference for a relative determination of the orbit. The absolute uncertainty of these measurements is basically determined by the uncertainty on the measurements made by Leinert et al. (1993), as quoted by the authors. The values published by Ghez, Neugebauer, & Matthews (1993) have been replaced by revised values published more recently (Ghez et al. 1995).

Figure 4 shows plots of the angular separations and position angles in Table 1 as a function of time, together with a least-square linear fit. Whereas the separation barely decreases, there is a clear variation in the position angle. As we shall see, assuming solar-like masses, the angular velocity is faster than one would expect for a circular orbit. Hence, the orbit must be eccentric and the stars near periastron. The binary pair rotates clockwise. From the millimetric CO band observations (Dutrey et al. 1994), we know that the east side of the disk is moving toward us. Assuming that the disk also rotates clockwise implies that we are viewing its south side.

From the fits in Figure 4, one can derive apparent separation $\boldsymbol{r}'$ and velocity $\boldsymbol{v}'$ vectors averaged over this 4.1 yr period of observations. In the following, we will assume that the distance of GG Tau is 140 pc (Elias 1987). This gives us

$$|\boldsymbol{r}'| = 35.6 \text{ AU}\,, \quad \arg(\boldsymbol{r}') = 2°.5\,,$$

$$|\boldsymbol{v}'| = 1.35 \text{ AU yr}^{-1}\,, \quad \arg(\boldsymbol{v}') = 255°\,,$$

where the argument (polar angle) is from north toward east. These vectors are projections on the sky plane of the true separation and velocity vectors. True orbital motion is very likely to take place in the same plane as the circumstellar ring. In the next section, we show that the ring axis of rotation makes an angle of 35° with the direction of obser-

TABLE 1

ORBITAL DATA

Date	Reference	Separation	Position Angle
1990 Nov 2	1	$0''.255 \pm 0''.010$	$9° \pm 2°$
1991 Oct 21	2	0.26 ± 0.01	2 ± 1
1993 Dec 26.....	3	0.26 ± 0.01	3 ± 2
1994 Sep 24	2	0.258 ± 0.004	357 ± 2
1994 Oct 18	2	0.242 ± 0.003	0.9 ± 0.5
1994 Dec 22.....	3	0.239 ± 0.005	357.2 ± 2

REFERENCES.—(1) Leinert et al. 1993. (2) Ghez et al. 1995. (3) This paper.

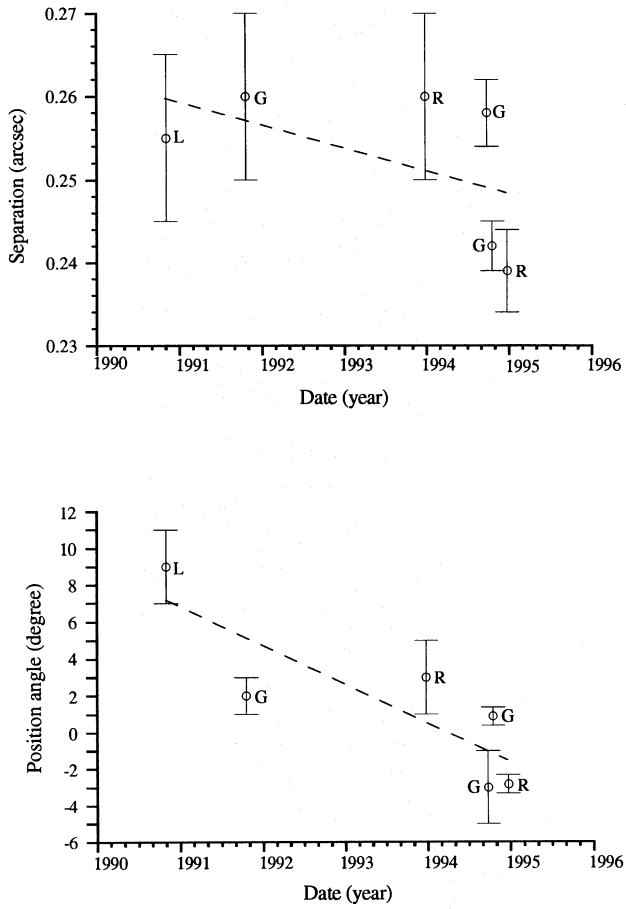

FIG. 4.—Linear fits to (*top*) the angular separations and (*bottom*) the position angles published in the literature. L = Leinert et al. (1993); G = Ghez et al. (1995); R = Roddier et al. (this paper).

vation, at a position angle of 20°. From these values, one can compute the true separation $\boldsymbol{r}$ and velocity $\boldsymbol{v}$ vectors. To do that, we take the position angle of 20° as a new origin for the polar angles, convert to rectangular coordinates, and divide the x-component by cos (35°). Converting back to polar coordinates give the following results:

$$|\boldsymbol{r}| = 42.8 \text{ AU}, \quad \arg(\boldsymbol{r}) = 345°,$$

$$|\boldsymbol{v}| = 1.45 \text{ AU yr}^{-1}, \quad \arg(\boldsymbol{v}) = 230°.$$

Taking these values as initial conditions, we have computed a family of orbits depending on the total mass M of the system. Table 2 shows the characteristics of these orbits.

Figure 5 shows the orbits projected back on the sky plane. We have estimated the radius of the circumbinary ring to be 220 AU (see § 5.2). If, following Dutrey et al. (1994), we admit that the ring radius is 2.7 times the semimajor axis of the binary orbit, then the total mass of the system must be of the order of 1.5–1.6 $M_\odot$. There is a large

TABLE 2

ESTIMATED ORBIT CHARACTERISTICS

Total Mass ($M_\odot$)	Semimajor Axis (AU)	Eccentricity	Period (yr)
1.4.....	111	0.72	1066
1.5.....	88	0.64	677
1.6.....	73	0.58	497

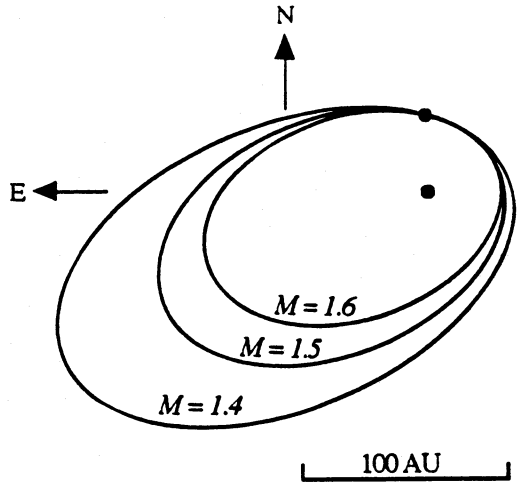

FIG. 5.—Estimated orbits for several values of the total mass M (in $M_\odot$).

uncertainty on this estimation. Including a 10% uncertainty on the distance of GG Tau (Elias 1978), the uncertainty on the velocity estimated from the data shown in Figure 4 is of the order of 20%. Since the system mass is proportional to the square of the velocity, the uncertainty on the mass is of the order of 40%. Hence, this result is not inconsistent with the total mass of 1.2 $M_\odot$ estimated from millimetric observations of the circumstellar gas motion (Dutrey et al. 1994).

5.2. *Circumbinary Ring*

A visual fit of an ellipse to the circumbinary ring gives a semimajor axis of 220 AU and a semiminor axis of 180 AU; that is, an average "radius" of 200 AU in fair agreement with the value of 160–180 AU estimated by Dutrey et al. (1994). The major axis of the ellipse forms an angle of 20° ± 2° with the east-west direction, again in good agreement with the value of 18° given by Dutrey et al. (1994). One can make a rough estimate of the location of the center of gravity of the binary system. If the ring is made of material in Keplerian motion, this center should be a focal point of an actual (unprojected) elliptical ring. Then, the ratio of its distance to the center of the ellipse over its distance to the ring (taken along the same radial direction) is $e(1 - e)^{-1}$, where e is the eccentricity of the actual ring. On the deconvolved images, we estimate this ratio to be 0.23, which yields $e = 0.18$. The corresponding ratio b/a of the actual semiminor axis over the actual semimajor axis of the elliptical ring is $b/a = (1 - e^2)^{1/2} = 0.98$. In other words, the ring is nearly circular with a radius equal to the semimajor axis of its projection on the sky, that is, 220 AU. The ratio 180/220 of the apparent semiminor axis over the semimajor axis is the cosine of the ring inclination, hence, an inclination angle of 35°, a value again similar to the 43° inclination quoted by Dutrey et al. (1994).

6. PHOTOMETRY

6.1. *Close Binary*

We did not attempt to estimate any absolute flux, only flux ratios. To determine flux ratios in binaries, we first tried the IRAF photometry package, but we found it unsatisfactory because turbulence-compensated stellar pro-

files do not match well Gaussian profiles, with or without circular symmetry. Since our stellar images are close to circular symmetry, we decided to estimate stellar profiles by taking azimuthal averages over circles centered on one star, but excluding a sector containing most of the light from the second star. The estimated circularly symmetric brightness distribution was then subtracted from the first star, and the flux of the remaining star was estimated through concentric circular apertures with increasing diameter. The procedure was applied to both components, and flux ratios were plotted as a function of the aperture diameters. Measurements were made both before and after deconvolution. In both cases, a plateau was observed beyond which ratios become affected by light mixing between components. Flux ratios from the plateau were found to be the same in both cases. Only deconvolved images produced a larger plateau.

All our photometric measurements are relative to the total flux from the close binary star. The results have then been converted into absolute fluxes using data on the binary published in the literature. There is a risk in doing so because of the known variability of the star. However, in the data we found in the literature (Rydgren, Schmelz, & Vrba 1982; Leinert et al. 1991; Hartigan, Strom, & Strom 1994), colors agree with each other within 0.1 mag, which is of the order of the uncertainty of our measurements. To minimize errors due to long-term variability, we took as a reference the most recent measurements of Hartigan et al. (1994) as given in Table 3.

Following Leinert et al. (1993), we will label the four stellar components of GG Tau as follows:

A.—Brighter component of the close (north) binary (0".25 separation).

a.—Fainter component of the close (north) binary (0".25 separation).

B.—Brighter component of the south binary (1".4 separation).

b.—Fainter component of the south binary (1".4 separation).

For each of these four stars, Table 4 gives the ratio of their brightness to that of the total brightness of the close binary (A + a). *J*-, *H*-, and *K*-band observations were made with standard filters. Observations noted as "*I* band" were actually made through a narrow-band filter centered at 0.85 μm. The quoted uncertainty indicates the dispersion of independent estimations. Using the magnitudes of the close binary shown in Table 3, one can now calculate magnitudes and colors for all four components. These are given in Table 5. The colors of the four GG Tau components are consistent with those published in the literature for classical T Tauri stars (Lada & Adams 1992). To estimate the true stellar luminosities, one has to correct the observe magnitudes from interstellar reddening. To do this, we used the extinction law of Rieke & Lebofsky (1985) and assumed an extinction coefficient $A_J = 0.35$ (Hartigan et al. 1994), the same for all components. The corrected magnitudes are given in Table 6. The related spectral energy distribution (SED) λF_λ (in W cm^{-2}) are given in Table 7 and plotted in Figure 6.

According to Hartigan et al. (1994) and others, the flux near 1 μm comes essentially from the star; hence, the $I-J$ color should reveal its spectral type. For this estimation, we used the colors given by Bessell & Brett (1988) with the following results:

1. Component A matches very well a K7-M0 star in the *I*, *J*, and *H* bands with some IR excess in the *K* band.
2. Component a matches a M4 star with IR excess in both *H* and *K* bands.
3. Component B matches a M5 star with no significant IR excess even in *K*.
4. Component b matches stars cooler then M6.

The uncertainty is $\pm$ one spectral type. Figure 6 shows for components A, a, and B, the estimated SED of the standard star which exactly matches the $I-J$ color. For these curves,

TABLE 3

MAGNITUDES OF THE CLOSE BINARY[a]

Band	Magnitude
I	10.25
J	8.90
H	8.07
K	7.53

[a] Hartigan et al. 1994.

TABLE 4

MEASURED FLUX RATIOS

Band	A	a	B	b
I	0.787 ± 0.006	0.213 ± 0.006	0.043 ± 0.005	0.0037 ± 0.0005
J	0.692 ± 0.003	0.308 ± 0.003	0.078 ± 0.005	0.0166 ± 0.0005
H	0.676 ± 0.003	0.324 ± 0.003	0.070 ± 0.005	0.0140 ± 0.0005
K	0.676 ± 0.005	0.324 ± 0.005	0.068 ± 0.005	0.0132 ± 0.0005

TABLE 5

DERIVED MAGNITUDES AND COLORS

Band	A	a	B	b
I	10.51	11.93	13.67	16.33
J	9.30	10.18	11.67	13.35
H	8.50	9.29	10.96	12.70
K	7.96	8.75	10.45	12.23
J−*H*	0.80	0.89	0.71	0.65
H−*K*	0.54	0.54	0.51	0.47

TABLE 6

UNREDDENED MAGNITUDES

Band	A	a	B	b
I	9.91	11.33	13.07	15.73
J	8.95	9.83	11.32	13.00
H	8.28	9.07	10.74	12.48
K	7.82	8.61	10.31	12.09

TABLE 7

SPECTRAL ENERGY DISTRIBUTIONS
λF_λ (10^{-16} W cm^{-2})

Band	A	a	B	b
I	0.77	0.21	0.042	0.0036
J	1.01	0.45	0.114	0.024
H	0.90	0.44	0.093	0.019
K	0.67	0.32	0.067	0.013

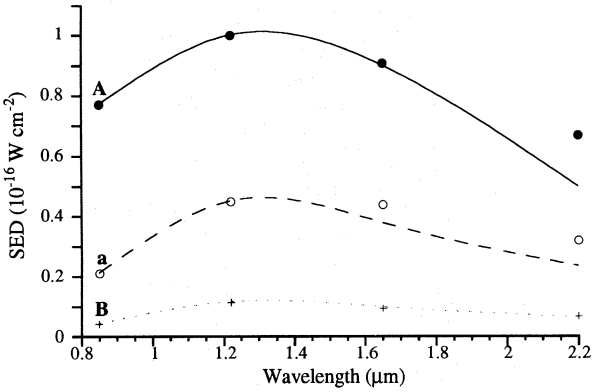

FIG. 6.—Observed spectral energy distribution (SED) for GG Tau A (*filled circles*), GG Tau a (*open circles*), and GG Tau B (*crosses*). Also shown are the SEDs of standard stars with the same $I-J$ magnitude: a K7-M0 star (*solid line*), an M3–4 star (*dashed line*), and an M5 star (*dotted line*). Note the IR excess in GG Tau A and GG Tau a.

we have interpolated the Bessell & Brett table between types. For component b, the uncertainty on the photometric measurements as well as the unavailability of models prevent us from doing so.

If these estimates are correct, then the binary pair (A, a) should show a 2.6 mag difference in the visible, in fair agreement with the 3 mag difference obtained recently from *HST* observations (White 1995). Hence, the visible spectrum of the binary should essentially be that of the A component. In the literature, it is classified either as M0 (Hartigan et al. 1994) or K7 (Strom et al. 1989b). The fact that we find an excellent match of component A with a standard star between K7 and M0 comforts us that the *I*, *J*, and *H* fluxes come essentially from the star. It means that most of the near-infrared excess that has previously been interpreted as coming from the disk (Rydgren et al. 1982; Shiba et al. 1993) comes in fact from the M4 star a. We still do find some IR excess for both components A and a. These excesses may come from warm inner disks surrounding each of these stars. If this interpretation is correct, then the fainter component a has a brighter inner disk than the brighter component A. In addition, there is no evidence of a warm disk around component B.

From these photometric results, one can estimate an effective temperature and a luminosity for each of the three components A, a, and B and put these stars in an H-R diagram. To do this, we used data from Table 4 of Hartigan et al. (1994). The resulting values are given here in Table 8. We have plotted these values against the theoretical evolutionary tracks used by Hartigan et al. (1994) and noted DM94 (D'Antona & Mazzitelli 1994), S94 (Swenson et al. 1994), and CK79 (Cohen & Kuhi 1979). This gave us the ages and masses shown in Table 9.

Although numbers vary widely from one model to the other, the stellar companion a appears to be systematically younger than the main star A, whereas the more remote component B appears to be of similar age, or older than, A. If this is correct, then it is interesting to note that the youngest star a has a warmer inner disk visible in both the *H* and *K* bands, the older star A has a cooler disk visible only in the *K* band, and the (probably) oldest star B shows evidence of a disk in neither the *H* nor the *K* band. We may see here the effect of the disk cooling down with time. The fact that a stellar companion a, only 40 AU away from the main star A, is about 10 times younger is surprising, since one would a priori expect A and a to be born together. Hartigan et al. (1994) has noted also that in one-third of his binary sample, the less massive star is younger than the more massive one. More recently, using speckle techniques, Koresko (1995) observed two close pairs, the spectra of which implies that the companion is younger. One possibility is that theoretical evolution tracks are affected by accretion (Hartmann & Kenyon 1990). However, evidence for accretion is often lacking or may be too episodic (Koresko 1995). Another more interesting possibility is that close stellar companions are produced by gravitational instabilities in circumstellar disks. This is known to be possible when the disk mass is at least similar to that of the central star (Adams, Ruden, & Shu 1989), which is indeed the case for GG Tau. A similar formation process has also been proposed for giant planets (Cameron 1985). If this is the case, one would expect the companion orbit to be nearly circular, which is not the case. However, Artymowicz & Lubow (1995) have shown recently that interactions between a binary and its circumbinary disk would rapidly increase the eccentricity of an initially circular obit. Therefore, we favor the latter interpretation. Moreover, evidence for instabilities can be seen in the lumpiness of the inner disks (see the following section).

For the close binary (A and a), the two most recent models (DM94 and S94) give a total mass ranging from 0.5 to 0.7 $M_\odot$, which is inconsistent with both the value of 1.2 $M_\odot$ estimated from gas motion (Dutrey et al. 1994) and our own value of 1.5 $M_\odot$ estimated from the binary orbital motion. The older model (CK79) gives $M_\odot$, which is only marginally consistent. It is difficult to explain this discrepancy. However, masses estimated from the H-R diagram do not include the inner disk masses. It may well be that the inner disks are massive enough to play a significant role in the gravitational pull on the orbiting material.

TABLE 8

EFFECTIVE TEMPERATURES AND LUMINOSITIES

Star	log $T_{\rm eff}$	log $L/L_{\rm solar}$
A.....	3.59	0.00
a	3.49	−0.12
B.....	3.48	−1.06

TABLE 9

AGES AND MASSES

	Age (yr)			Mass ($M_\odot$)		
Star	DM94	S94	CK79	DM94	S94	CK79
A.....	3×10^5	10^6	5×10^5	0.35	0.50	0.70
a	3×10^4	10^5	10^5	0.15	0.20	0.20
B.....	3×10^5	5×10^6	2×10^6	0.10	0.35	0.25

6.2. *Circumbinary Ring*

We have estimated both the fraction of light coming from the ring and its color. In doing this, we have first isolated a central zone containing 99% of the flux. This zone is roughly 1″ long in the north-south direction and 0.″6 wide in the east-west direction. Inside this zone, the flux comes essentially from the two stars and serves us as a calibration source. Then we have delimited the ring zone as extending between two concentric ellipses with the same $b/a = 0.82$ ratio and with semimajor axes of 1.″25 and 1.″90. We have

estimated the total flux coming from the ring zone and divided it by the flux coming from the central zone. For the three J, H, and K bands, we found the following flux ratios R:

$$R_J = 0.43 \times 10^{-2} \pm 0.12 \times 10^{-2} ,$$
$$R_H = 0.78 \times 10^{-2} \pm 0.08 \times 10^{-2} ,$$
$$R_K = 0.57 \times 10^{-2} \pm 0.25 \times 10^{-2} .$$

The error bar is given by the uncertainty in the deconvolution process. Note the large uncertainty in the K-band measurements which are affected by the sky background noise. Compared to the color of the central stars, the estimated color excesses are

$$E(J-H) = -2.5 \log (R_J/R_H) = 0.65 ,$$
$$E(H-K) = -2.5 \log (R_H/R_K) = -0.34 .$$

Light scattered by small dust particles is expected to be bluer than, or at least of the same color as, the illuminating source. Hence, compared to the H band, the lack of light from the ring in the J band is surprising. It means that light from the central stars must have been absorbed and therefore reddened before illuminating the ring. From the photometry of the central stars (§ 6.1), we found evidence for an IR excess produced by warm inner disks. The light we receive from the stars does not cross these disks. However, the light which illuminates the ring is likely to cross these disks (Cameron 1985; Ruden & Lin 1986). If light crosses the disks, it may be heavily absorbed. Assuming absorption by standard interstellar dust particles (Rieke & Lebofsky 1985), a $J-H$ color excess of 0.65 corresponds to an absorption $A_V = 6$ mag in the visible. If this is the case, then the ring will not be seen in the visible. Note that our CCD images did not show the ring. Recently recorded *HST* images do not show the ring either (Ghez 1995). Further evidence that such an absorption occurs will be given below.

A problem with this interpretation is that the ring has a brightness excess in H compared to K, whereas a reddening would have the opposite effect. To explain this discrepancy, one must consider first that part of the starlight we see in the H and K bands comes from the warm inner disks (IR excess). We see them almost face on. But viewed from the ring, the inner disks are seen edge on and contribute far less to the illumination. One can correct the above values from this effect by assuming that the inner disks have a negligible contribution to the ring illumination. If we replace the observed central source magnitudes by that of the stars alone (the spectra of which are shown in Fig. 6), we obtain the following corrections:

$$\Delta J = J_{\rm star} - J_{\rm (star+disk)} = 0 ,$$
$$\Delta H = H_{\rm star} - H_{\rm (star+disk)} = 0.044 ,$$
$$\Delta K = K_{\rm star} - K_{\rm (star+disk)} = 0.318 .$$

Hence, we obtain the new color excesses

$$E'(J-H) = E(J-H) - \Delta J + \Delta H = 0.69 ,$$
$$E'(H-K) = E(H-K) - \Delta H + \Delta K = -0.07 .$$

While these new values ease the problem, they do not fully solve it. A possible explanation is that ring particles have micron rather than submicron sizes. Then, their scattering efficiency may be similar in the J and H band and start to drop only in the K band. A similar phenomenon has been noted by Beckwith et al. (1990), who find spectral indices smaller than unity. Still another possibility is that, owing to the larger background noise, we have underestimated the K flux in the ring.

To investigate light variations in the ring, we have divided the ring zone into 24 sectors, 15° wide. For each of these subzones, we have estimated the flux as a function of the number of iterations of the deconvolution algorithm. Good to fair convergence was observed in both the J and H bands. Poorer results were obtained in the K band. By comparing the flux inside each sector to the flux through the central zone, we have estimated the sector brightness in magnitude per arsec^2. Figure 7 shows a plot of the observed J magnitudes as a function of the H magnitudes, together with the line of constant color $J-H = 0.83$, the color of the central illuminating source. It confirms that light scattered by the circumstellar material is mostly redder than that from the central source; that is, $J-H$ is larger. In addition, it shows that the J magnitude increases faster than the H magnitude; that is, the $J-H$ color is an increasing function of H. It demonstrates clearly that color variations are related to changes in the illumination, rather than changes in the properties of the scattering material. A uniform color would give a slope of unity. Here the slope is larger than unity, indicating that fainter regions are redder and confirming that light from the central source is absorbed and reddened with a reddening proportional to extinction. The slope of the J versus H curve gives the ratio of the A_J over A_H extinction coefficients. A least-square fit to the plot in Figure 7 gives a slope of 1.51 comparable to the ratio $A_J/A_H = 1.61$ for typical interstellar dust (Rieke & Lebofsky 1985). Hence, brightness variations along the ring seem mostly attributable to variations in the dust illumination, rather than variations in the dust density.

Additional evidence has been found by studying the azimuthal variations of brightness on each side of the ring. To do that, we have delimited two new zones we call the cavity and the outer disk. The cavity is the area between the central zone and the ring. The outer disk is an area extending beyond the ring, from the ring outer edge up to a concentric ellipse with a semimajor axis of 2.″6. Again, we have divided these areas into 24 sectors and measured their brightness as a function of the azimuth angle, starting from the west in a counterclockwise direction. Fair convergence of the deconvolution algorithm was observed in both H and J. Figure 8 shows a plot of the J magnitudes per arcsec^2 as a

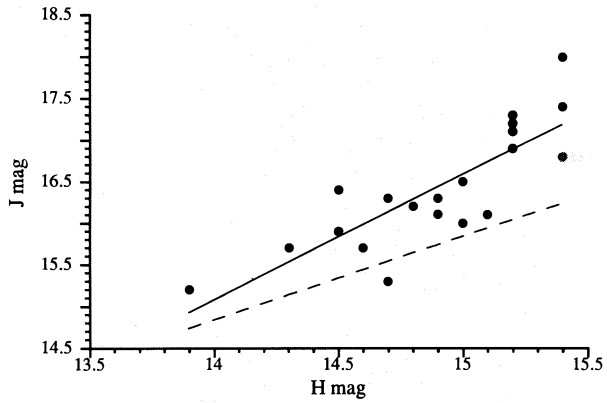

FIG. 7.—Observed J and H magnitudes per arcsec^2 along the ring. Solid line is a linear fit to the data. Dashed line is the line of constant color $J-H = 0.83$, the color of the central stars.

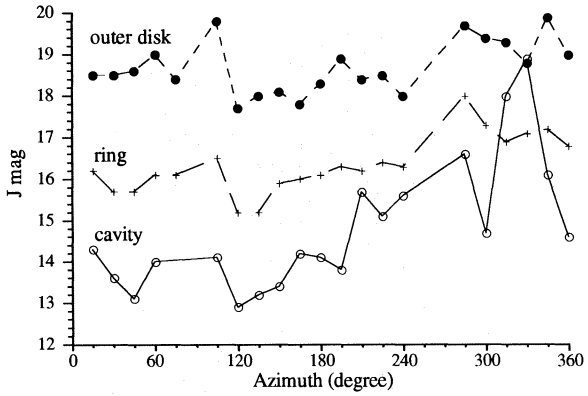

FIG. 8.—J magnitudes per arcsec^2 as a function of azimuthal angle in the cavity, the ring, and the outer disk. Uncertainties are of the order of 0.3–0.5 mag. Azimuthal angle is measured counterclockwise from west.

function of the azimuthal angle for each of the three zones: cavity, ring, and outer disk. Uncertainties are of the order of 0.3–0.5 mag. It is clear from this plot that intensity variations are well correlated. Since there is no a priori reason to believe that the azimuthal distribution of dust should be similar in the three zones, one must conclude again that the observed variations are due to changes in the illumination from the central stars. This means that at least the disk surrounding the main star has a nonuniform thickness. Figure 8 shows that there is systematically more light shining in the northeast direction, implying that the northeast part of the disk is thinner than the southwest part. It also shows well-correlated small-scale variations as if the disk was lumpy and/or contained holes. These nonuniformities are reminiscent of the arcs and clumps found recently in planetary rings (Ferrari & Brahic 1994; Showalter 1995). They may well be the product of resonant interaction with the companion. The bright spoke extending from the stars to the ring in the northeast direction may be produced by a beam of light shining through a hole in the disk. It is almost unreddened and visible on the CCD frames. We note also larger brightness variations in the cavity compared to the outer areas, as if dust was blown out of the holes, enhancing the cavity brightness. Perhaps under the influence of the companion, the disk around the main star has started to condense into large lumps, a possible first step toward planetary formation (Cameron 1985). A harmonic analysis of the azimuthal variations of the illumination show that most of the power is in the large-scale asymmetry. The remaining power is an order of magnitude lower and distributed mainly among even (symmetric) terms such as harmonics 2, 4, 6, and 8.

To study the radial distribution of dust, we have also divided the images into different zones delimited by concentric ellipses, and we have estimated the integrated flux into each zone. This has been done again as a function of the number of iterations of the deconvolution algorithm. Good to fair convergence was observed in all three wave bands. We have plotted the average amount of light scattered by the dust as a function of the radial distance expressed in AU. As long as the dust is optically thin, one can correct for the inverse square law of the illumination as a function of distance and obtain an estimate of the radial distribution of dust. This estimate is shown in Figure 9, where the three curves obtained in the J, H, and K bands have all been normalized to unity at maximum. Given the uncertainties in

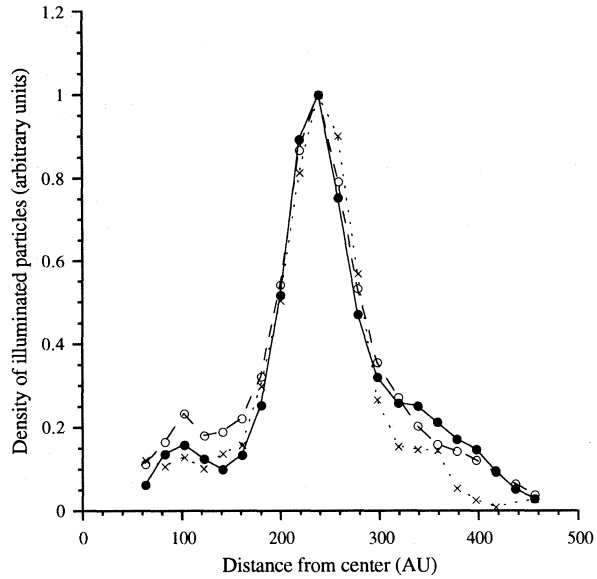

FIG. 9.—Average density profile of illuminated particles estimated by multiplying the square of the source distance by the amount of light scattered in the J band (*filled circles*), H band (*open circles*), and K band (*crosses*). Differences are within the estimated uncertainties.

the flux estimates, there is no significant difference between these curves. They give an average ring radius of 220 AU and an average width of 70 AU along the radial direction. As discussed below, the ring is probably optically thick in its plane, and the 70 AU width represents the optical depth over which light penetrates into the outer disk.

7. RING THICKNESS AND TEMPERATURE

From the above-described results, one can estimate the ring scattering solid angle

$$\Omega = \frac{S}{r^2}, \tag{1}$$

where S is the total cross section of the ring particles and r is the ring radius. Let $P_{\rm star}$ be the total radiative power emitted in the H band by the central stars. The power scattered by the ring is

$$P_{\rm ring} = \alpha k \frac{\Omega}{4\pi} P_{\rm star}, \tag{2}$$

where α is the dust albedo, and k is the inner disk absorption coefficient in the H band. In the last section, we have estimated the fraction R_H of light scattered by the ring in the H band. This fraction is

$$R_H = \frac{P_{\rm ring}}{P_{\rm star}} = \alpha k \frac{\Omega}{4\pi} = 0.78 \times 10^{-2}. \tag{3}$$

A 0.69 mag $J-H$ color excess (§ 6.2) corresponds to an extinction $A_H = 1.13$ mag, that is, an absorption coefficient $k = 0.35$. Assuming an albedo of $\alpha \leq 0.5$, the maximum value being typical for interstellar particles (Allen 1973, p. 264), one obtains a minimum scattering solid angle $\Omega = 0.56$.

If the ring is optically thick along the direction of propagation of light, all the light is intercepted by the ring and

$$\Omega = \frac{2\pi r h}{r^2} \geq 0.56, \tag{4}$$

where h is the thickness of the ring in a direction perpendicular to the light beam. This gives us a minimum thickness-to-distance ratio $h/r = 0.09$ in excellent agreement with the maximum value of 0.1 expected from theory (Ruden & Lin 1986). If the albedo was smaller than 0.5 and/or the ring was optically thin, then its thickness h would be larger than the expected maximum thickness. This leads us to two conclusions. First, the albedo must be quite high, typical of interstellar material rather than interplanetary material. Second, the ring must be optically thick, with a geometrical thickness

$$h \cong 0.1r = 20 \text{ AU} . \quad (5)$$

Hence, the ring represents only the inner rim of a hollow disk we call the outer disk. Light from the central source penetrates through the rim into the disk only up to a depth of 70 AU (§ 6.2). One should note that whereas the disk is optically thick in the direction of propagation of light, it is optically thin in a direction parallel to its axis.

The bolometric power absorbed by a perfectly black spherical particle of radius a located in the ring is

$$p = \frac{a^2}{4r^2} L , \quad (6)$$

where L is the luminosity of the central source in watts. We assume here that the energy absorbed by the inner disks is isotropically reradiated; therefore, p may be overestimated. The power radiated by the same particle is

$$p' = 4\pi a^2 \sigma T^4 , \quad (7)$$

where T is the particle temperature and σ is the Stefan-Boltzmann constant. At equilibrium, the powers p and p' are equal, giving

$$T = \left(\frac{L}{16\pi r^2 \sigma} \right)^{1/4} . \quad (8)$$

From Table 8, the sum of the luminosities of the two stars is $L = 1.76 L_{\text{solar}} = 6.68 \times 10^{26}$ W. This gives $T = 24$ K. The result is true for perfectly black or uniformly "gray" particles. As stated above, it may be overestimated. Nevertheless, we will take it as a crude estimate of the temperature of the particles in the ring. One can calculate their blackbody emission at wavelengths of 1.3 mm and 2.6 mm. One finds

$$B_\nu = 3.05 \times 10^{-16} \text{ W m}^{-2} \text{ Hz}^{-1} \text{ rad}^{-2} \quad \text{at 1.3 mm} ,$$

$$B_\nu = 8.63 \times 10^{-17} \text{ W m}^{-2} \text{ Hz}^{-1} \text{ rad}^{-2} \quad \text{ar 2.6 mm} .$$

If we assume that the total emitting area is the ring particle cross section S, then the flux F_ν received on Earth is

$$F_\nu = \frac{S}{d^2} B_\nu , \quad (9)$$

where d is the distance to Earth. Beckwith et al. (1990) give $F_\nu = 593 \pm 53$ mJy at 1.3 mm. Dutrey et al. (1994) give $F_\nu = 8.5$ mJy at 2.6 mm. Hence, one can have a new estimate of the ring scattering solid angle as

$$\Omega = \frac{S}{r^2} = \frac{F_\nu}{B_\nu} \left(\frac{d}{r} \right)^2 . \quad (10)$$

With $d = 140$ pc, $r = 220$ AU, and the above values of B_ν and F_ν, one obtains $\Omega = 0.42$ at 1.3 mm and $\Omega = 0.21$ at 2.6 mm, values consistent with our above estimate $\Omega = 0.56$, especially if we allow for a particle emissivity which decreases as the wavelength inverse (Beckwith et al. 1990). Hence, the particles seen in the near-infrared must also be the particles responsible for the millimeter emission.

8. SUMMARY

Our findings can be summarized as follows. The close binary pair rotates clockwise with an angular velocity of about 2 deg yr^{-1}. It implies that it is near the periastron of an eccentric orbit and that the total mass is of the order of 1.5 $M_\odot$. Photometry shows that the main star is a K7-M0 star with 1 $L_\odot$, whereas the companion is an M4 star with 0.76 $L_\odot$. Comparison with theoretical evolution tracks indicates that the companion must be 10 times younger than the main star, and that it was probably born inside a massive disk surrounding the main star. The same comparison gives a total stellar mass of the order of 0.5–0.7 $M_\odot$, which is inconsistent with the mass deduced from orbital velocities. Photometry shows that both stars have an IR excess, implying that they are both surrounded by a warm disk, the mass of which may explain at least part of this discrepancy.

Light from the central stars is clearly scattered along an apparently elliptical ring which surrounds them. Assuming that light is scattered by particles in Keplerian motion leads to the conclusion that the ring is nearly circular with a radius of 220 AU. Its axis is inclined by 35° from the line of sight. The direction of the axis is 20° east from north. The ring is redder than the central stars, the faintest parts being the reddest. This indicated that light which illuminates the ring has probably been absorbed and reddened by the inner disks which have been found to surround each star. If this is the case, then at least the disk which surrounds the main star is lumpy and more opaque in the southwest direction. Comparison with theoretical models of circumbinary disks (Artymowicz & Lubow 1995) leads to the conclusion that the ring must be the outer rim of a cavity formed by tidal interaction of a large disk with the orbiting binary. From the amount of scattered light, the thickness of the disk was estimated to be about one-tenth of its radius, in good agreement with theoretical estimates. Beyond the cavity rim, the disk is optically thick. Light penetrates into the disk only up to a distance of about 70 AU. Assuming that the illuminated particles reach a temperature of 24 K gives a millimeter continuum emission entirely consistent with the observations.

Note added in manuscript.—New adaptive optics observations of GG Tau were made by us at the CFHT, on 1995 November 20. The close binary was measured again, using the positions of the south components as a calibration. Assuming no uncertainty on these positions, we find a separation of 0.″23 ± 0.″1, and a position angle of 356.°5 ± 0.°5. These new values are fully consistent with those obtained on 1994 December 22 using the same calibration, and with the orbital velocity estimated in § 5.1.

The Cassegrain-focus adaptive optics instrument was built under NSF grant AST-9319004. The observing program is supported by NASA grant NAGW-4650. We wish to thank Hans Zinnecker for his constant guidance and encouragements. We are indebted to both Hans Zinnecker and Alan Tokunaga for kindly reviewing the manuscript before submission. We also acknowledge very helpful discussions with André Brahic and Pawel Artymowicz.

REFERENCES

Adams, F. C., Ruden, S. P., & Shu, F. H. 1989, ApJ, 347, 959
Allen, C. W. 1973, Astrophysical Quantities (3d ed.; London: Athlone)
Artymowicz, P., & Lubow, S. H. 1994, ApJ, 421, 651
———. 1995, in Disks and Outflows around Young Stars, ed. H. J. Staude & S. Beckwith (Berlin: Springer), in press
Beckwith, S., Zuckerman, B., Skrutskie, M. F., & Dyck, H. M. 1984, ApJ, 287, 793
Beckwith, S. V. W., Sargent, A. I., Chini, R. S., & Güsten, R. 1990, AJ, 99, 924
Bessell, M. S., & Brett, J. M. 1988, PASP, 100, 1134
Cameron, A. G. W. 1985, in Protostars & Planets II, ed. D. C. Black & M. S. Matthews (Tucson: Univ. Arizona Press), 1073
Cohen, M., & Kuhi, L. V. 1979, ApJS, 41, 743 (CK79)
D'Antona, F., & Mazzitelli, I. 1994, ApJS, 90, 467 (DM94)
Dutrey, A., Guilloteau, S., & Simon, M. 1994, A&A, 286, 149
Elias, J. H. 1978, ApJ, 224, 857
Ferrari, C., & Brahic, A. 1994, Icarus, 111, 193
Ghez, A. 1995, private communication
Ghez, A. M., Neugebauer, G., & Matthews, K. 1993, AJ, 106, 2005
Ghez, A. M., Weinberger, A. J., Neugebauer, G., Matthews, K., & McCarthy, D. W. 1995, AJ, 110, 753
Grasdalen, G. L., Strom, S. E., Strom, K. M., Capps, R. W., Thompson, D., & Castelaz, M. 1984, ApJ, 283, L57
Hartigan, P., Strom, K. M., & Strom, S. E. 1994, ApJ, 427, 961
Hartmann, L. W., & Kenyon, S. J. 1990, ApJ, 349, 190
Kawabe, R., Ishiguro, M., Omodaka, T., Kitamura, Y., & Miyama, S. M. 1993, ApJ, 404, L63
Kitamura, Y., Omodaka, T., Kawabe, R., Yamashita, T., & Handa, T. 1993, PASJ, 45, L27
Koerner, D. W., Sargent, A. I., & Beckwith, S. V. W. 1993, ApJ, 408, L93
Koresko, C. D. 1995, ApJ, 440, 764
Lada, Ch. J., & Adams, F. C. 1992, ApJ, 393, 278
Leinert, Ch., Haas, M., Richichi, A., Zinnecker, H., & Mundt, R. 1991, A&A, 250, 407
Leinert, Ch., Zinnecker, H., Weitzel, N., Christou, J., Ridgway, S. T., Jameson, R., Haas, M., & Lenzen, R. 1993, A&A, 278, 129
Lin, D. N., & Papaloizou, J. C. B. 1993, in Protostars and Planets III, ed. E. H. Levy & J. I. Lunine (Tuscon: Univ. Arizona Press), 749
Myers, P. C., Fuller, G. A., Mathieu, R. D., Beichman, C. A., Benson, P. J., Schild, R. E., & Emerson, J. P. 1987, ApJ, 319, 340
Rieke, G. H., & Lebofsky, M. J. 1985, ApJ, 288, 618
Roddier, F., Anuskiewicz, J., Graves, J. E., Northcott, M. J., & Roddier, C. 1994, Proc SPIE, 2201, 2
Roddier, F., Northcott, M., & Graves, J. E. 1991, PASP, 103, 131
Roddier, F., Roddier, C., Graves, J. E., & Northcott, M. J. 1995, ApJ, 443, 249
Ruden, S. P., & Lin, D. N. C. 1986, ApJ, 308, 883
Rydgren, A. E., Schmelz, J. T., & Vrba, F. J. 1982, ApJ, 256, 168
Sargent, A. I., & Beckwith, S. 1987, ApJ, 323, 294
Shiba, H., Sato, S., Yamashita, Y., Kobayashi, Y., & Takami, H. 1993, ApJS, 89, 299
Showalter, M. R. 1995, Science, 267, 490
Simon, M., & Guilloteau, S. 1992, ApJ, 397, L47
Skrutskie, M. F., et al. 1993, ApJ, 409, 422
Stapelfeldt, K. R., et al. 1994, BAAS, 26, 883
Strom, S. E., Edwards, S., & Strom, K. M. 1989a, in The Formation and Evolution of Planetary Systems, ed. H. A. Weaver & L. Danly (Cambridge: Cambridge Univ. Press), 91
Strom, K. M., Strom, S. E., Edwards, S., Cabrit, S., & Skrutskie, M. F. 1989b, AJ, 97, 1451
Swenson, J. H., Faulkner, J., Rogers, F. J., & Iglesias, C. A. 1994, ApJ, 425, 286 (S94)
White, R. 1995, in NATO-ASI Workshop on Evolutionary Processes in Binary Stars, Cambridge, UK, in press